SIAM J. SCI. COMPUT.
Vol. 21, No. 3, pp. 1066–1084

AXISYMMETRIC VORTEX SHEET MOTION: ACCURATE EVALUATION OF THE PRINCIPAL VALUE INTEGRAL*

MONIKA NITSCHE†

Abstract. This paper concerns the accurate evaluation of the principal value integral governing axisymmetric vortex sheet motion. Previous quadrature rules for this integral lose accuracy near the axis of symmetry. An approximation by de Bernadinis and Moore (dBM) that converges pointwise at the rate of $O(h^3)$ has maximal errors near the axis that are $O(h)$. As a result, the discretization error is not smooth. It contains high wavenumber frequencies that make it difficult to resolve the vortex sheet motion. This paper explains the reason for the degeneracy near the axis and proposes a modified quadrature rule that is uniformly $O(h^3)$. The results are based on an analytic approximation of the integrand, whose integral can be precomputed. The modification is implemented at negligible additional cost per timestep. As an example, it is applied to compute the evolution of an initially spherical vortex sheet.

Key words. vortex sheets, boundary integral methods, numerical integration

AMS subject classifications. 65D30, 76C05

PII. S1064827596314182

1. Introduction.

This work is motivated by an open question regarding the formation of singularities in vortex sheet evolution. It is known that planar vortex sheets with analytic initial data develop singularities in finite time [10], [13], [14], and [19], and that the singularity type is generic for all planar sheets [6]. One would like to know which types occur in three-dimensional (3D) sheets. To address this issue numerically, it is necessary to compute the vortex sheet motion accurately. In particular, one needs to resolve the high wavenumbers which determine the singularity type. This paper concerns the accurate evaluation of axisymmetric vortex sheet motion.

We consider closed vortex sheets that cross the axis of symmetry. An example is the sheet that induces flow past a sphere, shown in Figure 1.1. Here, x is the axis of symmetry. The vortex sheet evolution is described by its cross section with the upper x-y plane, $(x(\alpha,t), y(\alpha,t))$, $\alpha \in [a,b]$, and by the initial velocity jump across this curve, the vortex sheet strength $\sigma(\alpha)$. For the spherical sheet,

$$x(\alpha,0) = \cos(\alpha), \quad y(\alpha,0) = \sin(\alpha), \quad \sigma(\alpha) = \sin(\alpha)/2, \quad \alpha \in [0,\pi]. \tag{1.1}$$

To compute the evolution the vortex sheet is discretized by $N+1$ circular vortex filaments corresponding to a uniform mesh in α,

$$\alpha_j = jh, \quad j = 0,\dots,N, \quad h = \pi/N. \tag{1.2}$$

The filaments are initially located at $(x(\alpha_j,0), y(\alpha_j,0))$ and evolve with the vortex sheet velocity. The axial and radial velocity components u, v are given by principal value integrals

$$u(\alpha_j,t) = \fint_0^\pi G^u(\alpha,\alpha_j,t)d\alpha, \quad v(\alpha_j,t) = \fint_0^\pi G^v(\alpha,\alpha_j,t)d\alpha, \quad \alpha_j \in [0,\pi]. \tag{1.3}$$

*Received by the editors December 27, 1996; accepted for publication (in revised form) July 9, 1998; published electronically December 3, 1999. This work was partially supported by NSF grant DMS-9408697 and by an industrial postdoctoral membership at the Institute for Mathematics and Its Applications at the University of Minnesota.
http://www.siam.org/journals/sisc/21-3/31418.html
† Department of Mathematics and Statistics, University of New Mexico, Albuquerque, NM 87131 (nitsche@math.unm.edu).

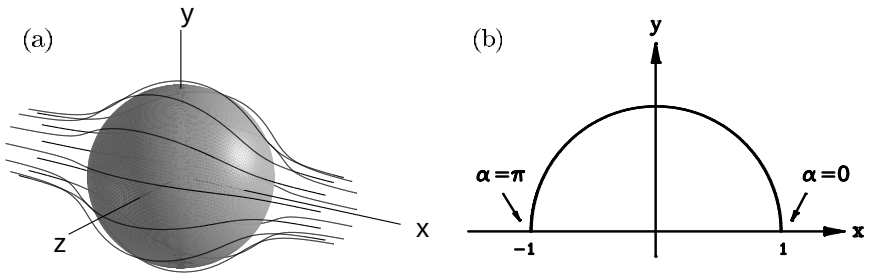

FIG. 1.1. *Axisymmetric vortex sheet inducing flow past a sphere.* (a) *3D perspective.* (b) *Curve representing the sheet in the symmetry plane.*

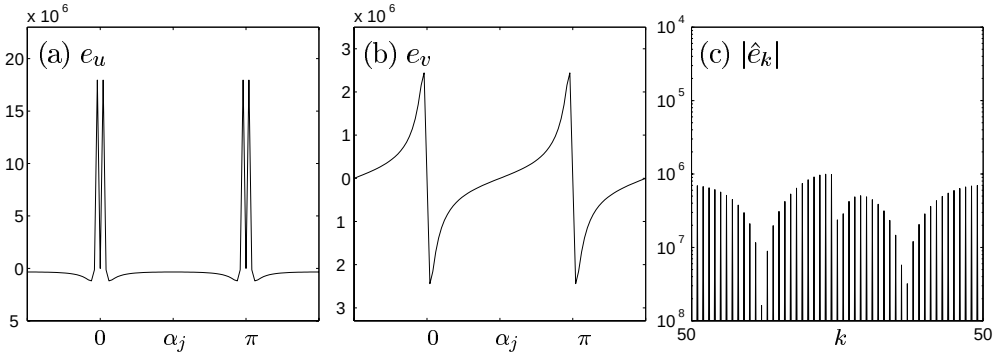

FIG. 1.2. *Error in the velocity (u, v) of the spherical vortex sheet* (1.1)*, computed using the dBM discretization with* $N = 50$*. The correct velocity is* (u_c, v_c)*.* (a), (b) *Periodic extension of the errors* $e_u = u_c - u, e_v = v_c - v$*.* (c) *Fourier coefficients* $\hat{e}_k$ *of the complex error* $e_u + ie_v$*.*

The integrands G^u, G^v, which will be specified later, have singularities at $\alpha = \alpha_j$ of the form $1/(\alpha-\alpha_j)$ and $(\alpha-\alpha_j)^k \log|\alpha-\alpha_j|$ for all $k \geq 0$. [20] discussed quadrature rules and the associated discretization errors for this type of equation. In the case considered in this paper, there is a difficulty that occurs near the axis of symmetry, when $\alpha_j \approx 0, \pi$.

This difficulty w as noted by dBM [5]. They proposed a discretization of (1.3) and applied it to the spherical vortex sheet (1.1), a good test case since the exact induced velocity is known [3, section 6.8]. Figure 1.2 plots the periodic extension of the discretization error (e_u, e_v) in the computed vortex filament velocity, using $N = 50$ filaments. Figures 1.2a, 1.2b show that in a thin region near the axis the discretization loses accuracy. As a result, the error is not smooth. Figure 1.2c plots the Fourier coefficients $\hat{e}_k$ of the complex error $e_u + ie_v$. It shows that the error contains high wavenumber frequencies of large amplitude. Pugh [18] used dBM's approximation to study singularity formation and found that the high modes in the error were too large to resolve the singularity type. He improved the accuracy near the axis using matched spherical harmonics expansions of the velocity but was unable to sufficiently smooth the error.

The loss of accuracy illustrated in Figure 1.2 is a general feature of closed axisymmetric interface problems. Lundgren and Mansour [12] used a boundary integral method proposed by [2] to compute the motion of liquid drops with surface tension and observed similar inaccuracies. Nie and Baker [16] circumvented the prob-

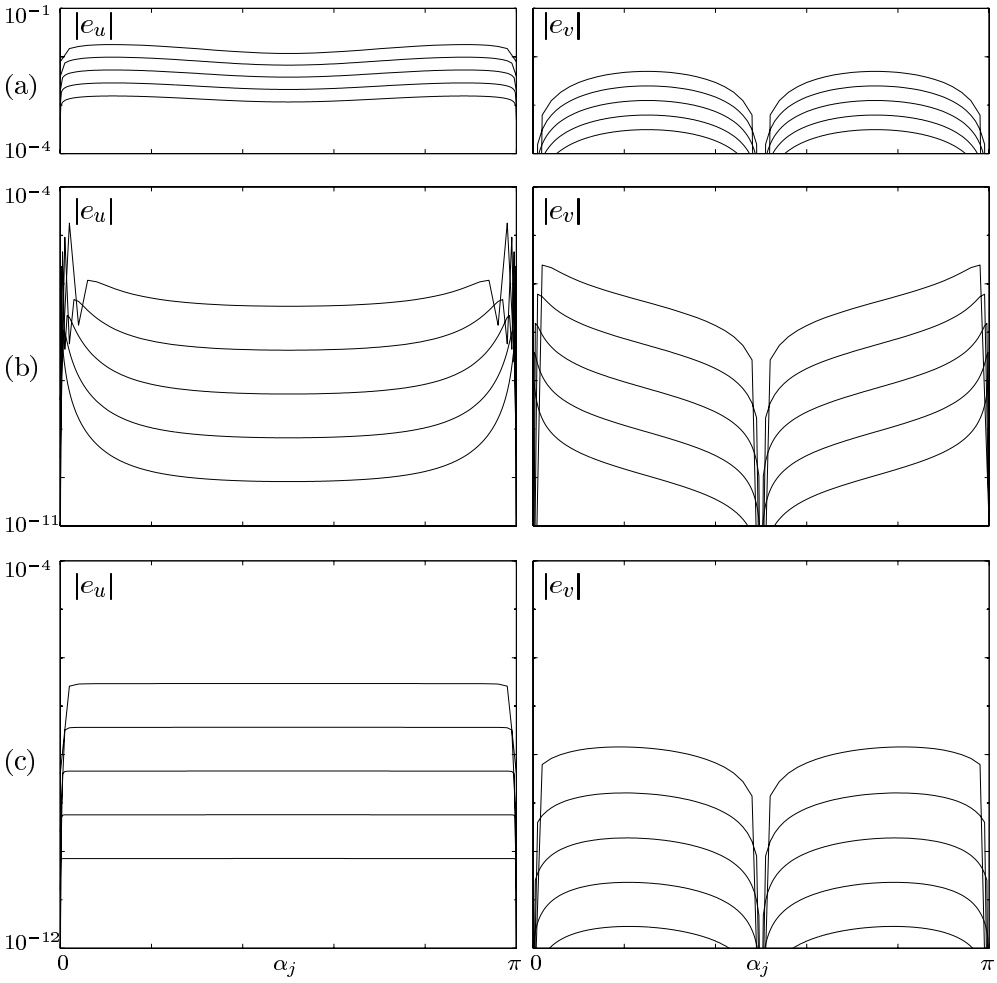

FIG. 1.3. *Errors* $|e_u|, |e_v|$ *in the velocity of the test case* (1.1)*, computed with* $N = 50, 100, 200, 400, 800$. (a) *Axisymmetric point vortex analogue.* (b) *dBM.* (c) *Modified dBM.*

lem using local mesh refinement. They interpolated the filament position at every timestep to a sufficiently fine mesh which is then used to evaluate the principal value integrals. The object of this paper is to explain the reason for the difficulty near the axis and to find a quadrature rule based on the $N + 1$ vortex filaments that is uniformly accurate. We remark that the difficulty discussed here is not present for axisymmetric sheets which remain far from the axis [8], nor for analogous planar vortex sheet problems.

The simplest approximation to (1.3) is the axisymmetric analogue of the point vortex approximation for planar sheets. The principal value integrals are approximated using the trapezoid rule, omitting the self-induced contribution of each vortex filament. The associated discretization error is $O(h \log h)$ [4], [20]. Figure 1.3a plots the error $|e_u|$ and $|e_v|$ using $N = 50, 100, 200, 400, 800$. It shows that the error decays slowly as N increases and that it is relatively large. Furthermore, the error is not smooth. Figure 1.4a plots the Fourier coefficients $\hat{e}_k$ of the error, with respect to a scaled wavenumber k/N. Here, only the even coefficients are plotted since for the

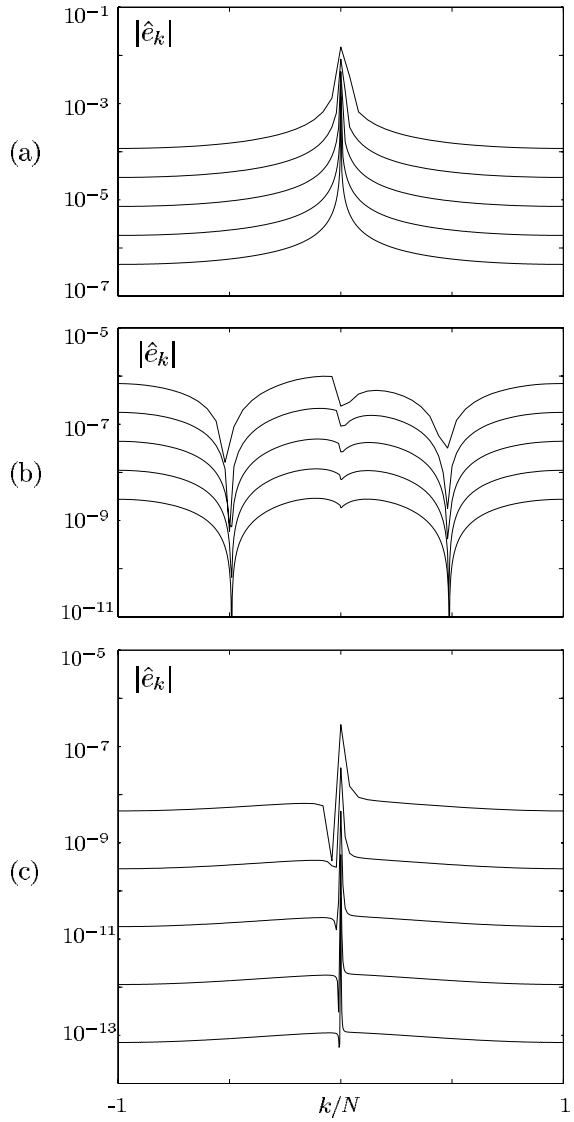

FIG. 1.4. *Fourier coefficients* $|\hat{e}_k|$ *of the complex error* $e_u + ie_v$ *in the test case* (1.1)*, computed with* $N = 50, 100, 200, 400, 800$*. Only the even coefficients are plotted.* (a) *Point vortex analogue.* (b) *dBM.* (c) *Modified dBM.*

test case (1.1), the odd ones are zero. The figure shows that the error contains high wavenumber frequencies of large amplitude. The largest mode $\hat{e}_N$ decays as $O(h^2)$. Note that this situation is different than in the planar case. The point vortex approximation for closed planar vortex sheets has a smooth discretization error with no high frequencies. This point is discussed further in [17].

In [5] dBM improve the point vortex analogue by extending van de Vooren's [21] correction for planar vortex sheets to the axisymmetric case. The correction consists of finding the unbounded singular components $1/(\alpha - \alpha_j)$ and $\log|\alpha - \alpha_j|$ of the integrand $G(\alpha, \alpha_j, t)$, integrating them exactly, and approximating the remainder by

the trapezoid rule. Figure 1.3b plots the associated discretization error for a range of values of N. For fixed α_j, the error decreases at the rate of $O(h^3)$, which follows from Sidi and Israeli's results [20]. However, the convergence rate does not hold uniformly and degenerates near the axis, $\alpha_j \approx 0, \pi$. We will show that the maximum error near the axis is $O(h)$. As a result, the discretization error remains nonsmooth. The Fourier coefficients of the error are plotted in Figure 1.4b. The amplitude of the high wavenumbers, albeit smaller than in 1.4a, does not decay any faster. The decay rate of $\hat{e}_N$ remains $O(h^2)$.

We will show that the reason for the degeneracy of dBM's approximation near the axis is that the derivatives of the integrand G at the endpoints as well as the constants multiplying the logarithmic singularities become unbounded as $\alpha_j \to 0, \pi$. These results will be derived from an analytic approximation of the exact integrand near the axis. We propose a modification to dBM's quadrature rule based on the approximate integrand. We subtract the approximate integrand from G, precompute its integral to machine precision, and integrate the remainder using dBM's approximation. Since the derivatives and relevant constants in the remaining integrand do not become unbounded as fast, the modified quadrature rule is uniformly $O(h^3)$. The error plotted in Figure 1.3c shows that the inaccuracies near the axis have been removed. The discretization error is also significantly smoother. The Fourier coefficients plotted in Figure 1.4c are smaller than in Figures 1.4a and b. Moreover, the amplitude of the high wavenumbers decays faster. In Figure 1.4c, $\hat{e}_N$ decays as $O(h^4)$.

The modification of dBM's approximation requires a minimal additional cost per timestep since the most costly component, the integration of the approximate integrand, is precomputed. As an example, we apply it to compute the evolution of the spherical sheet (1.1).

The paper is organized as follows. Section 2 presents the discretization of dBM [5] and the associated discretization error. Section 3 describes the approximation of the original integrand, its properties, and the error in the approximation. Section 4 describes how to modify dBM's discretization using the approximate integrand. The modification is applied to the initially spherical sheet in section 5. The results are summarized in section 6.

2. dBM's quadrature rule.

2.1. The exact integrand. As described in the introduction, the axisymmetric vortex sheet $(x(\alpha,t), y(\alpha,t))$, $\alpha \in [0,\pi]$, is discretized by $N+1$ vortex filaments at $(x(\alpha_j,t), y(\alpha_j,t))$ corresponding to a uniform mesh in α. The velocity of the jth filament is given by (1.3), where

$$G(\alpha,\alpha_j,t) = \sigma(\alpha)\mathcal{G}(x(\alpha,t), y(\alpha,t), x(\alpha_j,t), y(\alpha_j,t)) \tag{2.1}$$

and $\mathcal{G}(x,y,x_j,y_j)$ is the velocity at (x_j,y_j) induced by an axisymmetric filament at (x,y) of unit strength (see [11, section 161]),

$$\mathcal{G}^u(x,y,x_j,y_j) = \frac{1}{2\pi\rho_2}\left[\, F(\lambda) \;-\; \frac{(x-x_j)^2 + y_j^2 - y^2}{\rho_1^2}\; E(\lambda)\right], \tag{2.2a}$$

$$\mathcal{G}^v(x,y,x_j,y_j) = \frac{1}{2\pi\rho_2}\frac{x-x_j}{y_j}\left[\, F(\lambda) \;-\; \frac{(x-x_j)^2 + y_j^2 + y^2}{\rho_1^2}\; E(\lambda)\,\right]. \tag{2.2b}$$

Here, $\rho_1^2 = (x-x_j)^2 + (y-y_j)^2$, $\rho_2^2 = (x-x_j)^2 + (y+y_j)^2$, $F(\lambda)$ and $E(\lambda)$ are the complete elliptic integrals of the first and second kind, and $\lambda^2 = 4yy_j/\rho_2^2$. The

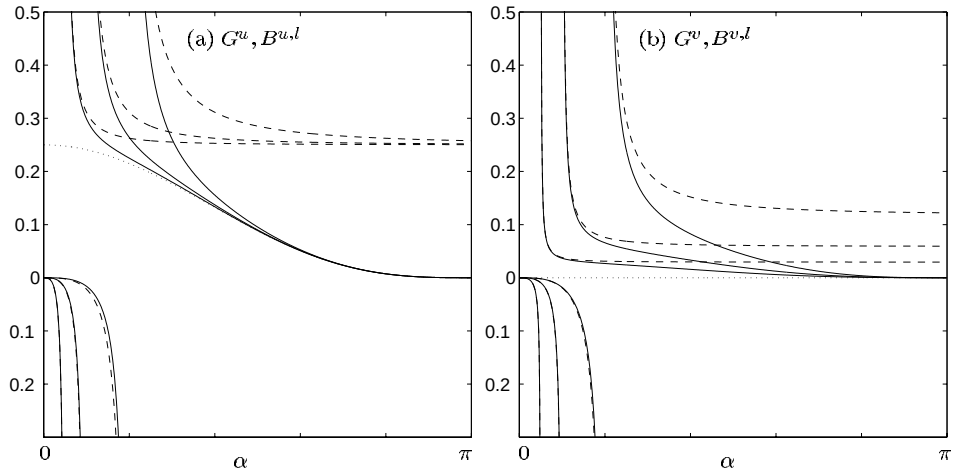

FIG. 2.1. *Exact integrand $G(\alpha, \alpha_j, 0)$ (solid curves) and approximate integrand $B^l(\alpha, \alpha_j, 0)$ (dashed curves) for $\alpha_j = \pi/5, \pi/10, \pi/20$. For reference, $G(\alpha, \alpha_j, 0)$ is also shown (dotted curve).* (a) *u-velocity.* (b) *v-velocity.*

superscripts u, v, refer to the axial and radial velocity components, respectively. The lack thereof, as in (2.1), implies that the expression applies to both u and v.

The integrand $G(\alpha, \alpha_j, t)$ for the test case (1.1) is plotted in Figure 2.1 for $\alpha_j = \pi/5$, $\pi/10$, $\pi/20$ (solid curves). As α_j decreases, the solid curves approach the limiting curve with $\alpha_j = 0$ (dotted curve). The dashed curves are plots of the approximate integrand and will be discussed later. The exact integrand G is singular at $\alpha = \alpha_j$. The form of the singularity is found using expansions of the elliptic integrals $F(\lambda)$ and $E(\lambda)$ for $\lambda \approx 1$ [1, section 17.3] and Taylor series expansions for $\alpha \approx \alpha_j$. One finds that

$$G(\alpha, \alpha_j, t) = G_o(\alpha, \alpha_j, t) + \frac{c_{-1}(\alpha_j, t)}{\alpha - \alpha_j} + \sum_{k=0}^{\infty} c_k(\alpha_j, t)\ (\alpha - \alpha_j)^k \log|\alpha - \alpha_j|, \tag{2.3}$$

where G_o is smooth.

The integral of the simple pole $c_{-1}/(\alpha - \alpha_j)$ is evaluated in the principal value sense. All the logarithmic singularities are integrable. The form of the coefficients c_k in the expansion (2.3) will be important for the results of this paper and will be discussed below. For reference, the first five coefficients c_k are given in the appendix.

2.2. Quadrature rule dBM. The integral of the two unbounded singularities of G,

$$J(\alpha, \alpha_j, t) = \frac{c_{-1}(\alpha_j, t)}{\alpha - \alpha_j} + c_0(\alpha_j, t)\ \log|\alpha - \alpha_j|, \tag{2.4}$$

can be evaluated numerically, but the associated error is large. However, the function J is time independent except for the factors c_{-1}, c_0. Up to these factors, its integral can therefore be precomputed exactly. This is analogous to van de Vooren's method for planar vortex sheets and is the main idea in dBM's approximation.

Here, we present a derivation of dBM's method which will motivate the results later in this paper. It is summarized in (2.5) below. The function J is defined on $\alpha \in (-\infty, \infty)$. The integrand $G(\alpha, \alpha_j, t)$ is extended from $\alpha \in [0, \pi]$ to $(-\infty, \infty)$

by zero. Subtract the unbounded component $J(\alpha,\alpha_j,t)$ from G on a large interval $[-L,L]$, integrate it exactly, and approximate the remaining integral by the trapezoid rule, as in (2.5a,b). Now rearrange the terms involving J and evaluate them in the limit $L\to\infty$, as in (2.5c),

$$\fint_0^\pi G d\alpha = \lim_{L\to\infty}\left[\int_{-L}^{L}(G-J)d\alpha + \fint_{-L}^{L} J d\alpha\right] \tag{2.5a}$$

$$\approx \lim_{L\to\infty}\left[h\sum_{k=-L/h}^{L/h}{}'(G-J)_k + \fint_{-L}^{L} J d\alpha\right] \tag{2.5b}$$

$$= h\sum_{\substack{k=0\\k\neq j}}^{N}{}' G_k + h(G-J)_j + \lim_{L\to\infty}\left[\fint_{-L}^{L} J d\alpha - h\sum_{\substack{k=-L/h\\k\neq j}}^{L/h}{}' J_k\right]. \tag{2.5c}$$

The reason for taking the limit $L\to\infty$ is to avoid errors in the trapezoid approximation in (2.5b) introduced by derivatives of J at the endpoints $\alpha=-L,L$. Furthermore, dBM found that the last term in (2.5c) can be evaluated in closed form in this limit.

The notation in (2.5) will be used throughout this paper. Integer subscripts k denote evaluation at $\alpha=\alpha_k$, with α_j,t fixed (for example, $J_k=J(\alpha_k,\alpha_j,t)$, $(G-J)_j=\lim_{\alpha\to\alpha_j}(G-J)(\alpha,\alpha_j,t)$). The prime on the summation indicates that the first and last summands are weighted by 1/2. The lack of superscript u, v denotes that the approximation applies to both velocity components. Furthermore, all derivatives that appear below (denoted by a dot, prime, or integer in brackets) are total derivatives with respect to α, unless otherwise specified.

The first term in (2.5c) is the axisymmetric analogue of the point vortex approximation. The middle term is given by

$$(G-J)_j^u = \frac{\sigma_j}{4\pi y_j}\left[\log\frac{8y_j}{f_j} - \frac{\dot{x}_j^2}{f_j^2}\right] + \frac{\dot\sigma_j\dot y_j}{2\pi f_j^2} + \frac{\sigma_j}{4\pi f_j^4}\left[\ddot y_j(\dot x_j^2-\dot y_j^2) - 2\dot x_j\dot y_j\ddot x_j\right], \tag{2.6a}$$

$$(G-J)_j^v = \frac{\sigma_j}{4\pi y_j}\left[-\frac{\dot x_j\dot y_j}{f_j^2}\right] - \frac{\dot\sigma_j\dot x_j}{2\pi f_j^2} + \frac{\sigma_j}{4\pi f_j^4}\left[\ddot x_j(\dot x_j^2-\dot y_j^2) + 2\dot x_j\dot y_j\ddot y_j\right], \tag{2.6b}$$

where $f_j^2=\dot x_j^2+\dot y_j^2$. The derivatives required to evaluate (2.6) are approximated numerically. The last term in (2.5) can be evaluated exactly in closed form, using Stirling's formula [5],

$$\lim_{L\to\infty}\left[\fint_{-L}^{L} J\ d\alpha - h\sum_{k\neq j}{}' J_k\right] = c_0(\alpha_j,t)\ h\log\frac{h}{2\pi}. \tag{2.7}$$

In summary, dBM's approximation with $h=\pi/N$ is

$$\fint_0^\pi G d\alpha\ \approx\ h\sum_{\substack{k=0\\k\neq j}}^{N}{}' G_k + h(G-J)_j + c_0(\alpha_j,t)\ h\log\frac{h}{2\pi} = dBM[G]_{[0,\pi]}^h. \tag{2.8}$$

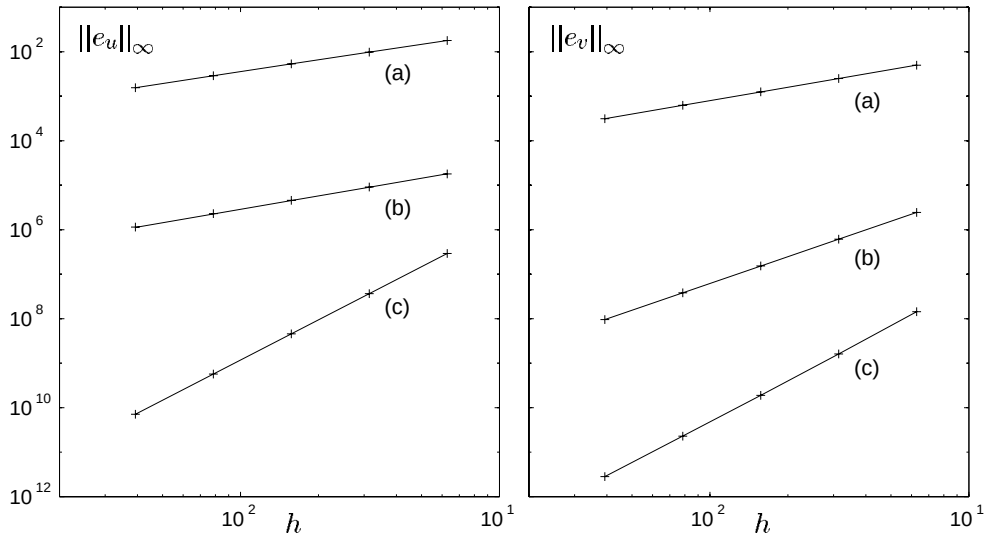

FIG. 2.2. *Maximum errors in the computed velocity (u, v) of the test case* (1.1) *versus* $h = \pi/N$. (a) *Point vortex analogue.* (b) *dBM.* (c) *Modified dBM. The crosses denote the computed values. The solid curves are* $e_u^a = -c_1 h \log h + c_2 h$, $e_v^a = c_3 h$, $e_u^b = c_4 h$, $e_v^b = c_5 h^2$, $e_u^c = c_6 h^3$, $e_v^c = c_7 h^3 + c_8 h^4$ $(c_{1,2} = 0.04, 0.17, c_3 = 0.08, c_4 = 0.0003, c_5 = 0.0006, c_{7,8} = 0.00005, 0.00019)$.

2.3. The error $\mathbf{E_{dBM}}$. The discretization error associated with the approximation (2.8) follows from Navot's work [15] and the results in [20]. It contains contributions from both the derivatives of G at the endpoints and the remaining logarithmic singularities in $G - J$. The odd derivatives $G^{(k)}(\alpha, \alpha_j, t)$ at $\alpha = 0, \pi$ contribute to errors of size h^{k+1}, as in the Euler–MacLaurin expansion (see [9, section 7.4]). In the present case only $k \geq 3$ contributes since the first derivative of G vanishes at the endpoints, $\alpha = 0, \pi$. This can be seen in Figure 2.1 for both G^u and G^v, and can be shown to hold at all times. The even logarithmic singularities remaining in $G - J$, $(\alpha - \alpha_j)^k \log|\alpha - \alpha_j|$, $k \geq 2$, contribute to errors of size h^{k+1}. The total discretization error has the form

$$
\begin{aligned}
E_{dBM}[G]_{[0,\pi]}^h &= \left[\fint_0^\pi G d\alpha - dBM[G]_{[0,\pi]}^h \right] \\
&= \sum_{\substack{k=3 \\ k \ odd}}^{\infty} \gamma_k \left[G^{(k)}(\pi, \alpha_j, t) - G^{(k)}(0, \alpha_j, t) \right] h^{k+1} + \sum_{\substack{k=2 \\ k \ even}}^{\infty} \nu_k c_k(\alpha_j, t) h^{k+1} \qquad (2.9) \\
&= O(h^3).
\end{aligned}
$$

The constants γ_k and ν_k are specified in [20, Proposition 2.29]. The expansion (2.9) of the discretization error neglects any errors in the approximation of the derivatives needed in (2.6), which are assumed to be sufficiently small.

The convergence rate $O(h^3)$ holds pointwise for fixed α_j. The results presented in Figures 1.2, 1.3b, however, suggest that the convergence rate does not hold uniformly in α_j. To confirm this, Figure 2.2 plots the maximal errors for the test case (1.1) versus the meshsize h, for the three approximations discussed in this paper: (a) the axisymmetric point vortex analogue, (b) the approximation by dBM, and (c) the modified dBM approximation. The least squares fit through the data points in Figure 2.2b (see caption) indicates that the maximal error in the u and v velocity components computed with dBM's approximation are $O(h)$ and $O(h^2)$, respectively.

The reason for the nonuniformity of dBM's approximation near the axis is the behavior of both the coefficients c_k and the derivatives $G^{(k)}$ near the endpoints, as $\alpha_j \to 0, \pi$. In the next section we show that

$$c_k^u(\alpha_j, t) \sim \frac{1}{\alpha_j^k}, \quad c_k^v(\alpha_j, t) \sim \frac{1}{\alpha_j^{k-1}} \tag{2.10}$$

and

$$G^{(k),u}(0, \alpha_j, t) \sim \frac{1}{\alpha_j^k}, \quad G^{(k),v}(0, \alpha_j, t) \sim \frac{1}{\alpha_j^{k-1}} \tag{2.11}$$

as $\alpha_j \to 0$. Substituting (2.10), (2.11) into (2.9) shows that if α_j is $O(h)$, then there are infinitely many contributions to the error of size h in the case of G^u, and of size h^2 in the case of G^v. The largest error, near the left endpoint, occurs when $\alpha_j = h$, that is, for $j = 1$. This can be seen in Figure 1.3b. Similar results hold near the right endpoint, when $\alpha_j \approx \pi$.

The results (2.10), (2.11) imply that one cannot alleviate the problem near the axis by approximating any finite number of the terms in the expansion (2.9) and removing them. The maximal error would always remain $O(h)$. In the next section we find an analytic approximation to the integrand G near each endpoint which approximates *all* of the terms in (2.9) to second order. We will use this fact to reduce the inaccuracies near the axis.

3. The approximate integrand.

3.1. Definition. This section presents the approximation B^l of G near the left endpoint $\alpha, \alpha_j \approx 0$. The approximation B^r of G near the right endpoint is obtained similarly and is not discussed here but is discussed in section 4 when we need it.

The approximation B^l is obtained using Taylor series about $\alpha, \alpha_j \approx 0$. The symmetry of the vortex sheet across the axis implies that the functions $x(\alpha, t), y(\alpha, t), \sigma(\alpha)$ have smooth extensions across $\alpha = 0$ defined by $x(-\alpha, t) = x(\alpha, t)$, $y(-\alpha, t) = -y(\alpha, t)$, $\sigma(-\alpha, t) = -\sigma(\alpha, t)$. It follows that for $\alpha \approx 0$,

$$\begin{aligned} x(\alpha, t) &= x_0(t) + \frac{\ddot{x}_0(t)}{2}\,\alpha^2 + O(\alpha^4), \\ y(\alpha, t) &= \dot{y}_0(t)\alpha + \frac{\dddot{y}_0(t)}{6}\,\alpha^3 + O(\alpha^5), \\ \sigma(\alpha) &= \dot{\sigma}_0\alpha + \frac{\dddot{\sigma}_0}{6}\,\alpha^3 + O(\alpha^5). \end{aligned} \tag{3.1}$$

Similar expansions hold for $x(\alpha_j, t), y(\alpha_j, t), \sigma(\alpha_j)$. In the remainder of this paper we assume that $\dot{y}_0 \neq 0$, that is, that the sheet crosses the axis at a right angle.

The exact integrand G is defined by (2.1) through the function $\mathcal{G}$. Let $\mathcal{H}(\xi, y, y_j), \xi = (x - x_j)^2$ be defined by (2.2) such that

$$\begin{aligned} \sigma\,\mathcal{G}^u(x, y, x_j, y_j) &= \frac{\sigma}{2\pi}\mathcal{H}^u(\xi, y, y_j), \\ \sigma\,\mathcal{G}^v(x, y, x_j, y_j) &= \frac{\sigma}{2\pi}(x - x_j)\mathcal{H}^v(\xi, y, y_j). \end{aligned} \tag{3.2}$$

The approximation B^l of G is defined using the first term of a Taylor expansion of $\mathcal{H}$

about the base point $(0, \dot{y}_0\alpha, \dot{y}_0\alpha_j)$,

$$
\begin{aligned}
G^v(\alpha,\alpha_j,t) &\approx B^{u,l}(\alpha,\alpha_j,t) = \frac{\dot\sigma_0}{2\pi}\,\alpha\,\mathcal{H}^u(0,\dot{y}_0\alpha,\dot{y}_0\alpha_j),\\
G^v(\alpha,\alpha_j,t) &\approx B^{v,l}(\alpha,\alpha_j,t) = \frac{\dot\sigma_0\ddot{x}_0}{4\pi}\,\alpha\,(\alpha^2-\alpha_j^2)\,\mathcal{H}^v(0,\dot{y}_0\alpha,\dot{y}_0\alpha_j).
\end{aligned}
\tag{3.3}
$$

We will first discuss the properties of B^l and then describe the form of the error in the approximation.

3.2. Properties. Figure 2.1 plots the approximate integrand $B^l(\alpha,\alpha_j,0)$ for $\alpha_j = \pi/5,\ \pi/10,\ \pi/20$ (dashed curve). Note that the first derivatives of both B^l and G vanish at the left endpoint and all the derivatives of B^l vanish as $\alpha\to\infty$.

The functions B^l plotted have an apparent self-similar structure: $B(\alpha,\pi/20,0)$ appears to be a rescaled version of $B(\alpha,\pi/10,0)$. One can indeed show that

$$
\begin{aligned}
B^{u,l}(\alpha,\alpha_j,t) &= b_0^{u}(t)\,B^{u,\star}\left(\frac{\alpha}{\alpha_j}\right), \qquad b_0^{u} = \frac{\dot\sigma_0}{2\pi\dot{y}_0},\\
B^{v,l}(\alpha,\alpha_j,t) &= \alpha_j b_0^{v}(t) B^{v,\star}\left(\frac{\alpha}{\alpha_j}\right), \quad b_0^{v} = \frac{\dot\sigma_0\ddot{x}_0}{4\pi\dot{y}_0^2},
\end{aligned}
\tag{3.4}
$$

for nondimensional functions

$$
\begin{aligned}
B^{u,\star}(\eta) &= \frac{\eta}{\eta+1}\,F(\lambda) + \frac{\eta}{\eta-1}\,E(\lambda),\\
B^{v,\star}(\eta) &= \eta\left[(\eta-1)\,F(\lambda) - \frac{\eta^2+1}{\eta-1}\,E(\lambda)\right].
\end{aligned}
\tag{3.5}
$$

Here, $\lambda^2 = 4\eta/(\eta+1)^2$.

Several properties of B^l can be deduced from the self-similar behavior (3.4). Just as G has an expansion of the form (2.3), $B^\star$ has the expansion

$$
B^\star(\eta) = B_o^\star(\eta) + \frac{c_{-1}^\star}{\eta-1} + \sum_{k=0}^{\infty} c_k^\star\,(\eta-1)^k\log|\eta-1|,
\tag{3.6}
$$

where $B_o^\star$ is smooth. The factors $c_k^\star$ are constants, independent of α_j or t. The first five of them are recorded in the appendix. Substituting $\eta = \alpha/\alpha_j$ one finds that B^l, given by (3.4), has an expansion of the form

$$
B^l(\alpha,\alpha_j,t) = B_o^l(\alpha,\alpha_j,t) + \frac{\tilde{c}_{-1}(\alpha_j,t)}{\alpha-\alpha_j} + \sum_{k=0}^{\infty}\tilde{c}_k(\alpha_j,t)\,(\alpha-\alpha_j)^k\log|\alpha-\alpha_j|,
\tag{3.7}
$$

where $\tilde{c}_k^u = b_0^{u}(t)c_k^{\star,u}/\alpha_j^k$ and $\tilde{c}_k^v = b_0^{v}(t)\alpha_j c_k^{\star,v}/\alpha_j^k$. It thus follows that

$$
\tilde{c}_k^u \sim \frac{1}{\alpha_j^k}, \quad \tilde{c}_k^v \sim \frac{1}{\alpha_j^{k-1}}.
\tag{3.8}
$$

This shows that (2.10) is satisfied if G is replaced by the approximate integrand B.

From the self-similar scaling behavior (3.4) it also follows by differentiation that the kth derivatives of B at the endpoint $\alpha = 0$ are

$$
B^{u,l(k)}(0,\alpha_j,t) \sim \frac{1}{\alpha_j^k}, \quad B^{v,l(k)}(0,\alpha_j,t) \sim \frac{1}{\alpha_j^{k-1}},
\tag{3.9}
$$

where k is odd and $k\ge 3$ since the first as well as all even derivatives of $B^\star$ at the endpoint vanish. Thus, (2.11) is satisfied if G is replaced by the approximate integrand B.

3.3. The error in the approximation. We would like to conclude from (3.8) and (3.9) that (2.10) and (2.11) is satisfied not only by the approximate integrand B but by the exact integrand G. To be able to do so, we need to know the form of the error in the approximation B of G. The error is obtained from Taylor series expansions of $\mathcal{H}$ and about the base point $(\xi, y, y_j) = (0, \dot{y}_0\alpha, \dot{y}_0\alpha_j)$ and $\alpha = 0$,

$$\begin{aligned} G^u(\alpha,\alpha_j,t) &= \frac{\sigma(\alpha)}{2\pi}\mathcal{H}^u(\xi(\alpha,\alpha_j,t), y(\alpha,t), y(\alpha_j,t)) \\ &= \frac{1}{2\pi}\left(\dot{\sigma}_0\alpha + \frac{\dddot{\sigma}_0}{6}\alpha^3\right)\Big[\mathcal{H}^u(0,\dot{y}_0\alpha,\dot{y}_0\alpha_j) \\ &\quad + \frac{\partial\mathcal{H}^u}{\partial y}(0,\dot{y}_0\alpha,\dot{y}_0\alpha_j)\frac{\dddot{y}_0}{6}\alpha^3 + \frac{\partial\mathcal{H}^u}{\partial y_j}(0,\dot{y}_0\alpha,\dot{y}_0\alpha_j)\frac{\dddot{y}_0}{6}\alpha_j^3 \\ &\quad + \frac{\partial\mathcal{H}^u}{\partial\xi}(0,\dot{y}_0\alpha,\dot{y}_0\alpha_j)\,\frac{\ddot{x}_0^2}{4}(\alpha^2-\alpha_j^2)\Big] + \text{h.o.t.} \end{aligned} \tag{3.10}$$

The first term on the right-hand side is the approximate integrand $B^{u,l}$. Let $H_1^u = \mathcal{H}^u$, $H_2^u = \partial\mathcal{H}^u/\partial y$, $H_3^u = \partial\mathcal{H}^u/\partial y_j$, and $H_4^u = \partial\mathcal{H}^u/\partial\xi$, evaluated at the base point. Then (3.10) reduces to

$$\begin{aligned} G^u(\alpha,\alpha_j,t) = B^{u,l}(\alpha,\alpha_j,t) + \frac{\dddot{\sigma}_0}{12\pi}\alpha^3 H_1^u(\alpha,\alpha_j,t) + \frac{\dot{\sigma}_0\dddot{y}_0}{12\pi}\Big[\alpha^4 H_2^u(\alpha,\alpha_j,t) \\ +\alpha\alpha_j^3 H_3^u(\alpha,\alpha_j,t)\Big] + \frac{\dot{\sigma}_0\ddot{x}_0^2}{8\pi}\alpha(\alpha^2-\alpha_j^2)^2 H_4^u(\alpha,\alpha_j,t) + \text{h.o.t.} \end{aligned} \tag{3.11}$$

It turns out that not only the first term but every term on the right-hand side of (3.11) can be expressed in terms of self-similar functions. After some algebraic manipulation, (3.11) is expressed as shown below in (3.12a). All factors $e_k(t)$ and functions $E_k^\star$ that appear are listed in the appendix. Similar results are obtained for G^v and are given in (3.12b):

$$(G^u - B^{u,l})(\alpha,\alpha_j,t) = \alpha_j^2\sum_{k=1}^{3} e_k^u(t)E_k^{\star,u}\Big(\frac{\alpha}{\alpha_j}\Big) + O(\alpha^4,\alpha_j^4) \tag{3.12a}$$

$$(G^u - B^{v,l})(\alpha,\alpha_j,t) = \alpha_j^3\sum_{k=1}^{4} e_k^v(t)E_k^{\star,v}\Big(\frac{\alpha}{\alpha_j}\Big) + O(\alpha^5,\alpha_j^5). \tag{3.12b}$$

The form of the error $G-B$ given by (3.12) is significant not only because it gives the next order correction to the approximation but because it suggests that the error itself is a sum of the form

$$G - B^l = \sum \alpha_j^k\, e_k(t)E_k\left(\frac{\alpha}{\alpha_j}\right), \tag{3.13}$$

where $k \geq 2$ in the case of G^u, and ≥ 3 in the case of G^v. If we make this assumption about the error terms $O(\alpha^4,\alpha_j^4), O(\alpha^5,\alpha_j^5)$ in (3.12), then differentiation of (3.12) shows that

$$\begin{aligned} \left(G^u - B^{u,l}\right)^{(k)}(0,\alpha_j,t) &= O(1/\alpha_j^{k-2}), \\ \left(G^v - B^{v,l}\right)^{(k)}(0,\alpha_j,t) &= O(1/\alpha_j^{k-3}). \end{aligned} \tag{3.14}$$

This estimate for the derivatives of the error, together with the estimate (3.9) for the derivatives of B, implies the estimate (2.11) for the derivatives of G. We have thus proven (2.11), under the assumption (3.13).

To show (2.10), we note that each of the functions $E^\star$ in (3.12), given in terms of elliptic integrals, can in turn be expanded in the form (3.6). It therefore appears that the left-hand side and the right-hand side of (3.12) have such an expansion. By equating coefficients, we obtain that

$$c_k^u - \tilde{c}_k^u = O(1/\alpha_j^{k-2}), \quad c_k^v - \tilde{c}_k^v = O(1/\alpha_j^{k-3}). \tag{3.15}$$

This result together with the estimate (3.8) for $\tilde{c}_k$ proves (2.10).

In summary, this section presented an approximation B^l from which we can deduce the unbounded growth (2.10), (2.11) of the coefficients and derivatives of G. Furthermore, the function B^l approximates all of these values to second order.

4. Modified dBM quadrature rule.

4.1. Quadrature rule for $\alpha_j \approx 0$. The nonuniformity in dBM's approximation arises from the unbounded growth (2.10), (2.11) of the coefficients and derivatives of G near the axis. The function B^l approximates all of these values to second order. Thus integration of $G - B^l$ should be more accurate than the integration of G. Moreover, B^l is time independent up to the factor b_o, and its integral can be precomputed. We therefore propose the following modification of dBM's approximation of (1.3).

The approximate integrand B^l is defined on $\alpha \in [0, \infty)$. The exact integrand G is extended from $\alpha \in [0, \pi]$ to $\alpha \in [0, \infty)$ by zero. We subtract the approximate integrand B^l from G on a large interval $[0, L]$, integrate it exactly, and approximate the remaining integral $G - B^l$ using dBM's approximation. We then rearrange the terms involving B^l and evaluate them in the limit $L \to \infty$. The proposed quadrature rule for $\alpha_j \approx 0$ is

$$\begin{aligned} \fint_0^\pi G d\alpha &= \lim_{L\to\infty} \left[\fint_0^L (G - B^l) d\alpha + \fint_0^L B^l d\alpha \right] \\ &\approx \lim_{L\to\infty} \left[dBM[B^l]_{[0,L]}^h + \fint_0^L B^l d\alpha \right] \\ &= dBM[G]_{[0,\pi]}^h + \lim_{L\to\infty} \left[\fint_0^L B d\alpha - dBM[B^l]_{[0,L]}^h \right] \\ &= dBM[G]_{[0,\pi]}^h + E_{dBM}[B^l]_{[0,\infty)}^h. \end{aligned} \tag{4.1}$$

This approximation equals dBM's quadrature rule plus a correction. The correction can be written in terms of the nondimensional functions $B^\star$, as follows:

$$\begin{aligned} E_{dBM}[B^{u,l}]_{[0,\infty)}^h &= b_0^u(t)\alpha_j E_{dBM}[B^{u,\star}]_{[0,\infty)}^{1/j}, \\ E_{dBM}[B^{v,l}]_{[0,\infty)}^h &= b_0^v(t)\alpha_j^2 E_{dBM}[B^{v,\star}]_{[0,\infty)}^{1/j}. \end{aligned} \tag{4.2}$$

Up to the factors $b_o(t)$, the correction (4.2) is time independent and can be precomputed. In order to evaluate $dBM[B^\star]$ as in (2.8), the following information is needed:

$$c_0^{\star,u} = -\frac{1}{2}, \quad c_0^{\star,v} = 0, \quad (B-J)_j^{\star,u} = 1 + \frac{1}{2}\log 8, \quad (B-J)_j^{\star,v} = -4, \tag{4.3}$$

where $J^\star$ contains the unbounded terms of $B^\star$.

The factors $b_o(t)$ depend only on the derivatives of x and y at one point, $\alpha = 0$. The vortex sheet is smooth at that point and the required derivatives can be evaluated accurately at a negligible cost. The correction to dBM's approximation is thus implemented at a minimal additional cost per timestep.

4.2. Quadrature rule for $\alpha_j \approx \pi$. The steps taken to approximate the integral of G near the right endpoint are analogous to the ones described for the left. Define

$$
\begin{aligned}
B^{u,r}(\alpha,\alpha_j,t) &= \frac{\dot\sigma_N}{2\pi}\,(\alpha-\pi)\,\mathcal{H}^u(x_N,\dot y_N(\alpha-\pi),x_N,\dot y_N(\alpha_j-\pi)),\\
B^{v,r}(\alpha,\alpha_j,t) &= \frac{\dot\sigma_N\ddot x_N}{4\pi}(\alpha-\pi)\big((\alpha-\pi)^2-(\alpha_j-\pi)^2\big)\\
&\quad\times\mathcal{H}^v(x_N,\dot y_N(\alpha-\pi),x_N,\dot y_N(\alpha_j-\pi)),
\end{aligned}
\tag{4.4}
$$

which can be written in terms of the function $B^\star$ given in (3.5) as

$$
\begin{aligned}
B^{u,r}(\alpha,\alpha_j,t) &= b_N^u(t)\,B^{u,\star}\left(\frac{\alpha-\pi}{\alpha_j-\pi}\right), \qquad b_N^u=\frac{\dot\sigma_N}{2\pi\dot y_N},\\
B^{v,r}(\alpha,\alpha_j,t) &= -(\pi-\alpha_j)b_N^v(t)B^{v,\star}\left(\frac{\alpha-\pi}{\alpha_j-\pi}\right), \quad b_N^v=\frac{\dot\sigma_N\ddot x_N}{4\pi\dot y_N^2}.
\end{aligned}
\tag{4.5}
$$

The quadrature rule that is accurate for $\alpha_j \approx \pi$ is

$$
\begin{aligned}
\fint_0^\pi G d\alpha &= \lim_{L\to\infty}\left[\fint_{-L}^{\pi}(G-B^r)d\alpha+\fint_L^\pi B^r d\alpha\right]\\
&\approx dBM[G]^h_{[0,\pi]}+E_{dBM}[B^r]^h_{(-\infty,\pi]}.
\end{aligned}
\tag{4.6}
$$

Approximation (4.6) equals dBM's quadrature rule plus a correction for $\alpha_j \approx \pi$. The correction can be written as

$$
\begin{aligned}
E_{dBM}[B^{u,r}]^h_{(-\infty,0]} &= b_N^u(t)(\pi-\alpha_j)E_{dBM}[B^{u,\star}]^{1/N-j}_{[0,\infty)},\\
E_{dBM}[B^{v,r}]^h_{(-\infty,0]} &= -b_N^v(t)(\pi-\alpha_j)^2E_{dBM}[B^{v,\star}]^{1/N-j}_{[0,\infty)}
\end{aligned}
\tag{4.7}
$$

and is precomputed except for the factors $b_N(t)$.

4.3. Uniformly accurate quadrature rule. To obtain a quadrature rule that is uniformly accurate for all $\alpha_j \in [0,\pi]$, we combine the left and right approximations in a weighted sum, as follows

$$
\begin{aligned}
\fint_0^\pi G d\alpha &\approx dBM[G]^h_{[0,\pi]}\\
&\quad + w_1(\alpha_j)E_{dBM}[B^l]^h_{[0,\infty)}+w_2(\alpha_j)E_{dBM}[B^r]^h_{(-\infty,\pi]}+q(\alpha_j,t)h^4\\
&= MdBM[G]^h_{[0,\pi]}.
\end{aligned}
\tag{4.8}
$$

The weights $w_1(\alpha_j)=\cos^2(\alpha_j/2)$ and $w_2(\alpha_j)=\sin^2(\alpha_j/2)$ are chosen so that they are positive, add up to one, vanish at one or the other endpoint, and are smooth and periodic. They introduce a second-order error at each endpoint, but this does not affect the size of the discretization error, as shown below.

The last term in (4.8) is a small correction for the u-velocity component given by the third derivatives of the integrand at the endpoints,

$$
q^u=\gamma_3(G^u-w_1B^{u,r})'''(\pi,\alpha_j,t)-(G^u-w_2B^{u,l})'''(0,\alpha_j,t), \quad q^v=0,
\tag{4.9}
$$

and $\gamma_3 = 1/720$. Although this term is of size $O(h^3)$ near the endpoints, it turns out to be slightly larger than the remaining $O(h^3)$ terms in the discretization error. We remove it in (4.8) in order to obtain cleaner results.

The discretization error associated with (4.8) is

(4.10)

$$\begin{aligned} E_{MdBM}[G]^h_{[0,\pi]} &= \left[\fint_0^\pi G d\alpha - MdBM[G]^h_{[0,\pi]} \right] \\ &= E_{dBM}[G]^h_{[0,\pi]} - w_1(\alpha_j) E_{dBM}[B^l]^h_{[0,\infty)} - w_2(\alpha_j) E_{dBM}[B^r]^h_{(-\infty,\pi]} - qh^4 \\ &= \sum_{\substack{k=3 \\ k\ odd}}^{\infty} \gamma_k \big[(G - w_1 B^r)^{(k)}(\pi, \alpha_j, t) - (G - w_2 B^l)^{(k)}(0, \alpha_j, t) \big] h^{k+1} \\ &\quad + \sum_{\substack{k=2 \\ k\ even}}^{\infty} \nu_k (c_k - w_1 \tilde{c}^l_k - w_2 \tilde{c}^r_k)(\alpha_j, t) h^{k+1} - qh^4. \end{aligned}$$

The error contains contributions from the derivatives of B^l at $\alpha = 0$, but none as $\alpha \to \infty$, since all the derivatives vanish in that limit. Similarly, it contains no contribution from the derivatives of B^r as $\alpha \to -\infty$. In the case of G^u, the correction qh^4 removes the first term in the expansion of the error.

Away from the endpoints, each one of the terms in the expansion (4.10) is $O(h^3)$. Near the endpoints, each term remains $O(h^3)$. For example, consider a term in the second series in (4.10) for $G = G^u$. Near the left endpoint, this term is

$$\nu_k(c^u_k - w_1 \tilde{c}^{u,l}_k - w_2 \tilde{c}^{u,r}_k) h^{k+1} = \nu_k \big((c^u_k - \tilde{c}^{u,l}_k) + (\alpha_j^2/4 + O(\alpha_j^4)) \tilde{c}^{u,l}_k - w_2 \tilde{c}^{u,r}_k \big) h^{k+1},$$

where we used that $w_1(\alpha_j) = 1 - \alpha_j^2/4 + O(\alpha_j^4)$. In view of (3.15), the first term on the right-hand side $\nu_k(c^u_k - \tilde{c}^{u,l}_k)h^{k+1}$ is $O(1/\alpha_j^{k-2})h^{k+1}$. In view of (3.8), the same holds for the second term. The last term on the right-hand side is $O(1)h^{k+1}$. Similar results hold for terms in the first sum in (4.10). Thus, if $\alpha_j = O(h)$, all of the terms in the expansion (4.10) are $O(h^3)$ for $G = G^u$. The same arguments apply to $G = G^v$. The expansion converges and the approximation is uniformly $O(h^3)$. Figure 1.3c, which plots the error $|e_u|$, $|e_v|$ for the test case (1.1), shows that the loss of accuracy near the axis has been removed.

It is possible to improve the convergence rate beyond $O(h^3)$ by removing the largest-order terms in the error (4.10). To that effect one needs a higher-order approximation B for G, given by the error terms listed in the appendix, higher-order weight functions w_1, w_2, the third derivatives at the endpoints, and the constants c_2 of both G and B.

4.4. Velocity on the axis. The approximation (4.8) holds at points α_j with $j \neq 0, N$, since neither B nor G are defined if $\alpha_j = 0, \pi$ or $y(\alpha_j) = 0$. That case is treated by taking the limit $\alpha_j \to 0, \pi$ in (2.1),

$$G^u(\alpha, \alpha_j, t) = \frac{\sigma}{2} \frac{y^2}{[(x - x_j)^2 + y^2]^{3/2}}, \quad G^v(\alpha, \alpha_j, t) = 0, \quad j = 0, N. \tag{4.11}$$

The integrands are plotted as dotted curves in Figure 2.1. Both integrands are bounded, even in the limit $(x, y) \to (x_j, 0)$. In this limit $\alpha \to \alpha_j$ and $G^u(\alpha, \alpha_j, t) \to \dot{\sigma}_j/(2\dot{y}_j), j = 0, N$. As a result, the integrals (1.3), for $j = 0, N$, are approximated using the trapezoid rule by

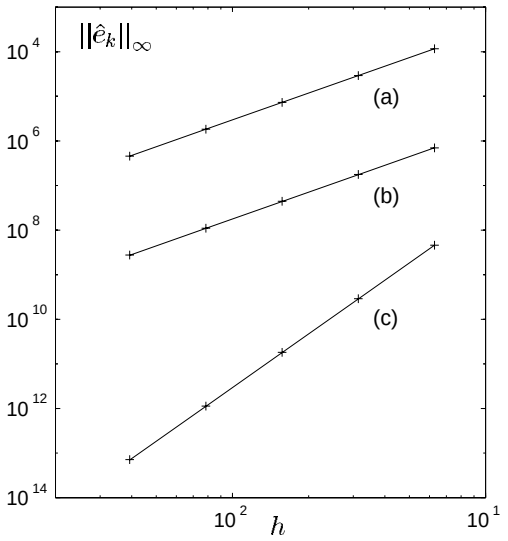

FIG. 4.1. *Fourier coefficient of the error with largest wavenumber, $|\hat{e}_N|$, versus $h = \pi/N$.* (a) *Point vortex analogue.* (b) *dBM.* (c) *Modified dBM. The crosses denote the computed values. The solid curves are $f_a = c_1 h^2$, $f_b = c_2 h^2$, $f_c = c_3 h^4$ ($c_1 = .03, c_2 = .0002, c_3 = .0003$).*

$$\int_0^\pi G^u(\alpha, \alpha_j, t) d\alpha \approx h \sum_{k=1}^{N-1} G^u_k + \frac{h}{4} \frac{\dot{\sigma}_j}{\dot{y}_j}, \quad \int_0^\pi G^v(\alpha, \alpha_j, t) d\alpha = 0, \quad j = 0, N. \tag{4.12}$$

All odd derivatives of G^u vanish at one endpoint, but the third derivative is nonzero at the other endpoint. Hence the approximation (4.12) is $O(h^4)$.

4.5. Comparison of PV analogue, dBM, and MdBM. Figures 1.3, 1.4, 2.2, and 4.1 compare the discretization error associated with (a) the point vortex analogue, (b) the approximation by dBM, and (c) the modified dBM approximation, using $N = 50, 100, 200, 400, 800$. The discretizations are applied to the test case (1.1).

Figure 1.3 plots the errors in the computed u- and v-velocity components, $|e_u|$, $|e_v|$ as a function of α_j, and has already been discussed. The maximal errors are plotted in Figure 2.2 versus h. Least squares approximations to the data are given in the caption. For the point vortex analogue, the maximal errors are $O(h \log h)$ and $O(h)$ for the u- and v-velocity, respectively. The $h \log h$ term arises from the largest logarithmic singularity in G^u which is absent in G^v, hence the difference in the convergence rates. For dBM's approximation, the maximal axial and radial errors are $O(h)$ and $O(h^2)$, as follows from (2.10), (2.11). In the modified dBM discretization the maximal errors are $O(h^3)$.

Figures 1.4 and 4.1 compare the Fourier coefficients $\hat{e}_k$ of the complex error, $(e_u + i e_v)_j = \sum_{k=-N}^{N} \hat{e}_k e^{ik\alpha_j}$, k even. Figure 1.4 shows that in all three discretizations, the error contains high nonzero Fourier modes, whose amplitude does not decay with k. The high modes are smallest in Figure 1.4c. The rate of convergence of the high modes is also fastest in Figure 1.4c. To estimate the rate of convergence, Figure 4.1 plots $|\hat{e}_N|$ versus $h = \pi/N$. The least squares fit to the data (see caption) shows that the decay is $O(h^2)$ in both the point vortex analogue and dBM's approximation, and $O(h^4)$ in the modified approximation.

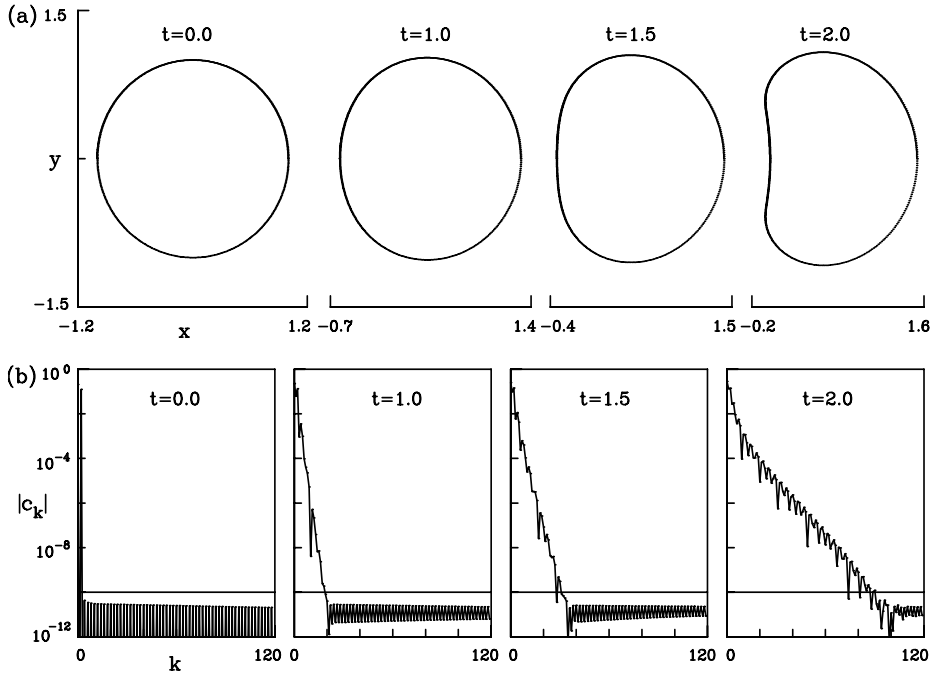

FIG. 5.1. *Time evolution, computed with* $N = 200$. (a) *Vortex sheet.* (b) *Fourier coefficients* $|c_k|$ *of the complex velocity* $u + iv$. *The horizontal line indicates the cut-off level for the filter.*

5. Time evolution. In order to describe details of the implementation of (4.8), this section applies the modified quadrature rule to compute the evolution of the spherical vortex sheet (1.2). The discrete system of ordinary differential equations

$$
\begin{aligned}
&dx_j/dt = MdBM[G^u]^h_{[0,\pi]}(\alpha_j, t),\\
&dy_j/dt = MdBM[G^v]^h_{[0,\pi]}(\alpha_j, t), \quad j = 1, \ldots, N-1,\\
&dx_j/dt = h \sum_{k=1}^{N-1} \frac{y_k^2\, \sigma_k}{2((x_k - x_j)^2 + y_k^2)^{3/2}} + \frac{h\dot{\sigma}_j}{4\dot{y}_j}, \quad dy_j/dt = 0, \quad j = 0, N,\\
&x_j(0) = \cos(\alpha_j), \quad y_j(0) = \sin(\alpha_j), \quad \sigma_j = \frac{1}{2}\sin(\alpha_j), \quad j = 0, \ldots N
\end{aligned}
\tag{5.1}
$$

is integrated in time using the Runge–Kutta method. The velocity computed at each stage of the method contains high Fourier modes introduced by the discretization error, as shown in Figure 1.4. To prevent the growth of these modes under the Kelvin–Helmholtz instability of the sheet, Krasny's Fourier filter [10] is applied to the vortex sheet velocity: all the Fourier modes in the velocity which are smaller than a preset upper bound τ are removed every time the velocity is computed. The filter level τ is chosen to be the amplitude of the largest mode in the computed velocity at $t = 0$ which is not present in the exact velocity.

Figure 5.1 shows that this filter level is sufficient to prevent the growth of the high modes. The figure plots the solution to (5.1) using $N = 200$ and timestep $\triangle t = 0.005$. Figure 5.1a shows the computed vortex sheet represented by the points $(x_j(t), y_j(t)), j = 0, \ldots, N$ and their images in the symmetry plane, at the indicated times. Figure 5.1b plots the corresponding Fourier coefficients of the complex velocity,

as well as the filter level $\tau = 10^{-10}$. The figure shows that the size of the modes introduced primarily by the discretization error remains bounded by their size at $t = 0$. Thus the filter level determined at $t = 0$ is sufficient to remove these modes at all times. As the number of points increases, the filter level can be reduced as $\tau(h) = O(h^3)$, and one obtains a sequence of solutions. Caflisch, Hou, and Lowengrub [7] recently analyzed the convergence of such a process.

6. Summary. The motion of closed axisymmetric vortex sheets is governed by a pair of principal value integrals (1.3) which are difficult to evaluate accurately. dBM proposed a quadrature rule which converges pointwise at the rate of $O(h^3)$, but near the axis, the maximal error is $O(h)$. As a result, the discretization error is not smooth. It contains high Fourier modes which grow under the Kelvin–Helmholtz instability of the sheet and preclude accurate computation of the vortex sheet motion.

This paper explains the reason for the loss of accuracy near the axis. The integrand contains logarithmic singularities of the form $c_k(\alpha - \alpha_j)^k \log|\alpha - \alpha_j|$ for all $k \geq 0$. The coefficients c_k and the odd derivatives of the integrand at the endpoints grow unboundedly as α_j approaches the axis of symmetry. They each introduce an error of size $O(h)$. The situation is different than for planar vortex sheets problems, where the integrand contains no logarithmic singularities.

We derive an analytic approximation to the axisymmetric integrand that approximates all of the unbounded terms to second order. By integrating this approximate integrand exactly, we modify dBM's quadrature rule and obtain a discretization that is uniformly $O(h^3)$. Without the inaccuracies near the axis, the computed velocity is sufficiently smooth to permit computations at high precision. This modification is implemented at a negligible additional cost per timestep, since the approximate integral can be precomputed. As an example, the modified quadrature rule is applied to compute the evolution of an initially spherical vortex sheet. The order of accuracy can be improved if desired using the information given in the Appendix.

Appendix. The coefficients $c_k(\alpha_j, t)$ in the expansion (2.3) of the integrand G are given by derivatives of $x(\alpha,t)$ and $y(\alpha,t)$ at $\alpha = \alpha_j$. The first five coefficients are

$$
\begin{aligned}
c^u_{-1} =& \frac{\sigma_j \dot{y}_j}{2\pi f_j^2}, \qquad c^u_0 = -\frac{\sigma_j}{4\pi y_j}, \qquad c^u_1 = \frac{1}{16\pi y_j^2}\,[-4\dot{\sigma}_j y_j + \sigma_j \dot{y}_j],\\
c^u_2 =& \frac{1}{64\pi y_j^3}\,[4y_j(\dot{\sigma}_j\dot{y}_j - 2\ddot{\sigma}_j y_j) + \sigma_j(3\dot{x}_j^2 - \dot{y}_j^2 + 2y_j\ddot{y}_j)],\\
c^u_3 =& \frac{1}{384\pi y_j^4}\,\Big[\, 4y_j^2(-4\dddot{\sigma}_j y_j + 3\ddot{\sigma}_j\dot{y}_j) + 6\dot{\sigma}_j y_j(3\dot{x}_j^2 - \dot{y}_j^2 + 2y_j\ddot{y}_j)\\
&\qquad + \sigma_j\left(18\dot{x}_j\ddot{x}_j y_j - \frac{81}{4}\dot{x}_j^2\dot{y}_j + \frac{3}{4}\dot{y}_j^3 - 6y_j\dot{y}_j\ddot{y}_j + 4y_j^2\dddot{y}_j\right)\Big],\\
c^v_{-1} =& -\frac{\sigma_j \dot{x}_j}{2\pi f_j^2}, \qquad c^v_0 = 0, \qquad c^v_1 = \frac{-3\sigma_j\dot{x}_j}{16\pi y_j^2},\\
c^v_2 =& \frac{-3}{32\pi y_j^3}\,[2y_j\dot{\sigma}_j\dot{x}_j + \sigma_j(\ddot{x}_j y_j - \dot{x}_j\dot{y}_j)],\\
c^v_3 =& \frac{1}{512\pi y_j^4}\,\big[\, -48y_j(\ddot{\sigma}_j\dot{x}_j y_j + \dot{\sigma}_j\ddot{x}_j y_j - \dot{\sigma}_j\dot{x}_j\dot{y}_j)\\
&\qquad + \sigma_j(15\dddot{x}_j - 16\dddot{x}_j\dot{y}_j^2 + 24\ddot{x}_j y_j\dot{y}_j - 21\dot{x}_j\dot{y}_j^2 + 24\dot{x}_j y_j\ddot{y}_j)\,\big],
\end{aligned}
$$

where $f_j^2 = \dot{x}_j^2 + \dot{y}_j^2$ and all derivatives (denoted by a dot) are taken with respect to α.

The coefficients $c_k^\star$ in expansion (3.6) of the nondimensional function $B^\star$ are constants. The first five are

$$c_{-1}^{\star,u} = 1, \quad c_0^{\star,u} = -1/2, \quad c_1^{\star,u} = -3/8, \quad c_2^{\star,u} = 3/32, \quad c_3^{\star,u} = -7/256,$$
$$c_{-1}^{\star,v} = -2, \quad c_0^{\star,v} = 0, \quad c_1^{\star,v} = -3/4, \quad c_2^{\star,v} = -3/4, \quad c_3^{\star,v} = 3/128.$$

The error in the approximation (3.3) of the exact integrand G by the approximate integrand B^l is given by (3.12) where the coefficients e_k and the functions $E_k^\star$ are

$$e_1^u(t) = \frac{\dddot{\sigma}_0}{12\pi\dot{y}_0}, \quad e_2^u(t) = \frac{\dot{\sigma}_0\dddot{y}_0}{12\pi\dot{y}_0^2}, \quad e_3^u(t) = \frac{\dot{\sigma}_0\ddot{x}_0^2}{16\pi\dot{y}_0^3}$$
$$e_1^v(t) = \frac{\dddot{\sigma}_0\ddot{x}_0}{24\pi\dot{y}_0^2}, \quad e_2^v(t) = \frac{\dot{\sigma}_0\ddot{x}_0\dddot{y}_0}{24\pi\dot{y}_0^3}, \quad e_3^v(t) = \frac{\dot{\sigma}_0\dddot{x}_0}{48\pi\dot{y}_0^2}, \quad e_4^v(t) = \frac{\dot{\sigma}_0\ddot{x}_0^3}{32\pi\dot{y}_0^4}$$
$$E_1^{\star,u}(\eta) = \eta^3\left[\frac{F(\lambda)}{\eta+1} + \frac{E(\lambda)}{\eta-1}\right],$$
$$E_2^{\star,u}(\eta) = -\eta\left[\frac{F(\lambda)}{\eta+1} - \frac{2\eta^2+1}{\eta-1}E(\lambda)\right],$$
$$E_3^{\star,u}(\eta) = \eta\left[(\eta-1)F(\lambda) - \frac{1+7\eta^2}{\eta-1}E(\lambda)\right],$$
$$E_1^{\star,v}(\eta) = \eta^3\left[(\eta-1)F(\lambda) - \frac{\eta^2+1}{\eta-1}E(\lambda)\right],$$
$$E_2^{\star,v}(\eta) = \eta\left[-(\eta-1)(\eta^2+2)F(\lambda) + \frac{\eta^4+9\eta^2+2}{\eta-1}E(\lambda)\right],$$
$$E_3^{\star,v}(\eta) = \eta(\eta^2+1)\left[(\eta-1)F(\lambda) - \frac{\eta^2+1}{\eta-1}E(\lambda)\right].$$
$$E_4^{\star,v}(\eta) = \eta\left[-(\eta-1)(\eta^2+1)F(\lambda) + \frac{\eta^4+14\eta^2+1}{(\eta-1)}E(\lambda)\right], \quad \lambda^2 = 4\eta/(\eta+1)^2.$$

Acknowledgments. I learned much about this problem from David Pugh's thesis. I thank Xiaofan Li, Gregory Kriegsman, and Michael Shelley for helpful comments and am especially grateful to Robert Krasny for carefully reading the manuscript and making many useful suggestions.

REFERENCES

[1] M. Abramowitz and I. A. Stegun, *Handbook of Mathematical Functions*, Dover, New York, 1965.

[2] G. Baker, D. I. Meiron, and K. H. Orszag, *Boundary integral methods for axisymmetric and three-dimensional Rayleigh–Taylor instability problems*, Phys. D, 12 (1984), pp. 19–31.

[3] G. K. Batchelor, *An Introduction to Fluid Mechanics*, Cambridge University Press, Cambridge, 1967.

[4] B. de Bernadinis, J. M. R. Graham, and K. H. Parker, *Oscillatory flow around disks and through orifices*, J. Fluid Mech., 102 (1981), pp. 279–299.

[5] B. de Bernadinis and D. W. Moore, *A ring-vortex representation of an axi-symmetric vortex sheet*, in Studies of Vortex Dominated Flows, M. Y. Hussaini and M. D. Salas, eds., Springer, New York, Berlin, 1987, pp. 33–43.

[6] R. E. Caflisch, N. Ercolani, T. Y. Hou, and Y. Landis, *Multi-valued solutions and branch point singularities for nonlinear hyperbolic or elliptic systems*, Comm. Pure Appl. Math., 46 (1993), pp. 453–499.

[7] R. E. Caflisch, T. Y. Hou, and J. Lowengrub, *Almost optimal convergence of the point vortex method for vortex sheets using numerical filtering*, Math. Comp., 68 (1999), pp. 1465–1496.
[8] R. E. Caflisch, X. Li, and M. J. Shelley, *The collapse of an axi-symmetric, swirling vortex sheet*, Nonlinearity, 6 (1993), pp. 843–867.
[9] G. Dahlquist and A. Björck, *Numerical Methods*, Prentice–Hall, Englewood Cliffs, NJ, 1974.
[10] R. Krasny, *A study of singularity formation in a vortex sheet by the point-vortex approximation*, J. Fluid Mech., 167 (1986), pp. 65–93.
[11] H. Lamb, *Hydrodynamics*, 6th ed., Dover, New York, 1932.
[12] T. S. Lundgren and N. N. Mansour, *Oscillations of drops in zero gravity with weak viscous effects*, J. Fluid Mech., 194 (1988), p. 479–510.
[13] D. I. Meiron, G. R. Baker, and S. A. Orszag, *Analytical structure of vortex sheet dynamics. 1. Kelvin-Helmholtz instability*, J. Fluid Mech., 114 (1982), pp. 283–298.
[14] D. W. Moore, *The spontaneous appearance of a singularity in the shape of an evolving vortex sheet*, Proc. Roy. Soc. London Ser. A, 365 (1979), pp. 105–119.
[15] I. Navot, *An extension of the Euler-Maclaurin summation formula to functions with a branch singularity*, J. Math. Phys., 40 (1961), pp. 271–276.
[16] Q. Nie and G. Baker, *Application of adaptive quadrature to axi-symmetric vortex sheet motion*, J. Comput. Phys., 143 (1998), pp. 49–69.
[17] M. Nitsche, *Singularity Formation and Roll-Up from a Cylindrical and a Spherical Vortex Sheet*, preprint, 1999.
[18] D. A. Pugh, *Development of vortex sheets in Boussinesq flows—Formation of singularities*, Ph.D. thesis, Imperial College of Science and Technology, London, 1989.
[19] M. J. Shelley, *A study of singularity formation in vortex sheet motion by a spectrally accurate vortex method*, J. Fluid Mech., 244 (1992), pp. 493–526.
[20] A. Sidi and M. Israeli, *Quadrature methods for periodic singular and weakly singular Fredholm integral equations*, J. Sci. Comput., 3 (1988), pp. 201–231.
[21] A. I. van de Vooren, *A numerical investigation of the rolling up of vortex sheets*, Proc. Roy. Soc. London Ser. A, 373 (1980), pp. 67–91.